Model calculation of the differential cross sections and angle-integrated cross sections of the emitted triton for neutron-induced ^{6}Li reactions at low incident energies

Jiaqi Hu,[1] Sheng Wang,[1,*] Xiaojun Sun,[2,1,†] Yinlu Han,[2,3] and Jingshang Zhang[3]

[1]*School of Nuclear Science and Technology, Xi'an Jiaotong University, Xi'an 710049, People's Republic of China*

[2]*College of Physics, Guangxi Normal University, Guilin 541004, People's Republic of China*

[3]*China Institute of Atomic Energy, P.O. Box 275(41), Beijing 102413, People's Republic of China*

(Received 2 February 2021; accepted 2 April 2021; published 22 April 2021)

Regarded as important for applications and theoretical studies, the differential cross sections of the emitted triton for the neutron-induced ^{6}Li reaction at low incident energies were calculated, based on the zero-range distorted-wave Born approximation theory with the assumption of ^{6}Li nucleus consisting of $t + ^3$He or $d + \alpha$. As a function of widths and excited energies of the discrete energy levels, an effective excited energy formula was proposed to describe their partial contributions. In addition, the optical model potential parameters, which had been successfully used to reproduce the double-differential cross sections of the emitted neutrons in our previous works in incident energy range from 5.0 to 20.0 MeV were extended in a low-energy range from 1.0 eV to 3.0 MeV in this paper. The calculated results agreed well with the measured differential cross sections recently published in 2020 and were further consistent with the measured angle-integrated cross sections. This indicates that the knock-out process and heavy-particle knockout process were dominant in an energy range from 1.0 eV to 3.0 MeV, whereas the shapes of the measured angular distributions in incident energy range from 0.1 to 1.0 MeV could be successfully explained by the Hauser-Feshbach model.

DOI: 10.1103/PhysRevC.103.044611

I. INTRODUCTION

Lithium isotope ^{6}Li is a structural material nucleus that plays an important role in the fields of nuclear technology and nuclear engineering. First, lithium is a major tritium breeding material in a thermonuclear fusion reactor system [1] whose performance is significantly affected by neutron-induced ^{6}Li reaction in its blankets. Second, the nuclear reaction data of the neutron-induced ^{6}Li reaction are widely used in neutron spectrometry and calibration of detectors [2]. The neutron-induced ^{6}Li reaction in the intermediate energy region (5.0–20.0 MeV) has been successfully calculated with the statistical theory of light nucleus reactions (STLN) [3–6] in our previous works [7], which, however, failed to explain the experimental data in the low incident energy region [7]. Therefore, further theoretical investigations in the low incident energy region are necessary to deepen the understanding of the light nucleus reaction mechanism. There are only (n, el), (n, γ), and (n, t) reaction channels opened at incident neutron energy below 1 MeV for the neutron-induced ^{6}Li reaction. Moreover, contribution from (n, t) reaction to total cross sections is dominant below 0.1 MeV. Thus, the knowledge of the (n, t) reaction is of great significance to the theoretical study of the neutron-induced ^{6}Li reaction at low bombarding energies.

There are many experimental data of the differential cross sections and angle-integrated cross sections for the ^{6}Li(n, t) reaction in experimental nuclear reaction data [8]. According to the new measurement reported in 2020 [9], the differential cross sections and angle-integrated cross sections for the ^{6}Li(n, t) reaction are given in incident neutron energy range from 1.0 eV to 3.0 MeV at 80 energy points. For 50 neutron energy points below 0.1 MeV, the experimental data of the differential cross sections for the ^{6}Li(n, t) reaction are systematically available for the first time in this energy region. These 50 energy points in the region from 1.0 eV to 0.1 MeV are distributed at equal logarithm intervals; 20 energy points in the region from 0.1 to 1.0 MeV are distributed at equal logarithm intervals to better display the resonance peak from 0.1 to 0.4 MeV; and ten energy points in the region from 1.0 to 3.0 MeV are distributed with an equal separation of 0.2 MeV. Below 0.01 MeV, the measured angle-integrated cross sections indicate a $1/v$ behavior. The resonance peak, which does not appear in the measured angle-integrated cross sections below 0.1 MeV, first shows up at around 0.24 MeV due to the 7.454-MeV energy level of the compound nucleus ^{7}Li.

The differential cross sections of the ^{6}Li(n, t) reaction based on the *R*-matrix code EDA [10] at energy below 4 MeV had been given in ENDF/B-VIII.0 [11] and JEFF-3.3 [12]. The cross sections of the ^{6}Li(n, t) reaction at energy up to 20 MeV were taken from the fitting of experimental data by using the *R*-matrix method in both libraries mentioned above. In JENDL-4.0 [13,14], the differential cross sections of the ^{6}Li(n, t) reaction were not given. The cross sections of the ^{6}Li(n, t) reaction were calculated with the *R*-matrix method below 1.0 MeV. Above 1.0 MeV, the experimental data were adopted, and the evaluation curve was determined by a least-squares method. The agreements of the results by the *R*-matrix method and

*shengwang@mail.xjtu.edu.cn

†sxj0212@gxnu.edu.cn

experiments demonstrate that the *R*-matrix method was able to fit the ^{6}Li(n,t) reaction but failed to clearly explain the reaction mechanisms. Therefore, a better understanding of the reaction mechanism for the ^{6}Li(n,t) reaction is necessary in the low-energy region.

In addition to the *R*-matrix method, several other theories were developed to analyze the ^{6}Li(n,t) reaction. A microscopic refined resonating group model calculation [15] that uses semirealistic N-N potentials has been performed to analyze the ^{6}Li(n,t) reaction. The cross-section resonances from this calculation are generally too broad and not always in the right positions [15]. The STLN [3–6] taking into account the preequilibrium mechanism, and the equilibrium mechanism has been successfully applied to calculate neutron-induced ^{6}Li reaction [7] in the incident energy range from 5.0 to 20.0 MeV because the preequilibrium mechanism is dominant in this energy region [4,6]. But the STLN failed to explain the cross sections with resonance structures at energy below 3.0 MeV [7]. Based on the assumption of deuteron exchange, the *S*-matrix theory has been applied to calculate the differential cross sections of the ^{6}Li(n,t) reaction. The obvious discrepancies between the calculated results from the *S*-matrix theory and the experimental data have been reported at low energies [16].

Newly measured differential cross sections [9] indicate that the anisotropy of the emitted triton is noticeable above 100 eV and that the angular distributions are markedly raised forward above 1 keV. So it is inspired that the direct reaction model may be applicable to analyze the differential cross sections of the emitted triton. Several light nucleus reactions [17–24] have been successfully analyzed by the direct reaction model based on the distorted-wave Born approximation (DWBA) theory. Furthermore, many studies, such as ^{12}C(d,p), ^{13}C(d,p), ^{13}C(d,t), and ^{13}C(d,α) reactions at $E_d = 0.41$–0.81 MeV [25], the ^{13}C(d,p) reaction at $E_d = 0.2$–0.35 MeV [26], the ^{12}C$(d,p\gamma)$ reaction at $E_d = 2.80$, 3.23, and 3.70 MeV [27], the ^{7}Li(d,d) and ^{7}Li(d,p) reactions at $E_d = 1.0$–2.6 MeV [28], and the ^{12}C(d,p) and ^{10}B(d,p) reactions below $E_d = 3.0$ MeV [29], indicate that the DWBA theory, under certain conditions, can be adopted to analyze the light nucleus reactions even in a relatively low incident energy region. Actually, the optical model potential (OMP) and the DWBA theory can be applied if the energy levels of the compound nucleus are broad enough to make appreciable overlapping, which means the cross sections may vary smoothly [25,30]. The cross sections of the ^{6}Li(n,t) reaction are, in fact, smooth at incident neutron energy below 0.1 MeV with no resonances. The energy levels of the compound nucleus ^{7}Li are broad except for the fourth and seventh energy levels in incident energy below 3.0 MeV. An effective excited energy formula, which is applied to describe the effects from the energy levels of the compound nucleus ^{7}Li, will be proposed and discussed later.

One of the first questions concerning the direct reaction model calculation is whether the mechanism is pickup or knockout. A pickup model [31,32] has been used to calculate the differential cross sections of the ^{6}Li(n,t) reaction for several neutron energies. The theoretical values of the differential cross sections for large angles are far too low. In some cases, the theoretical values of the differential cross sections for large angles can be improved if the knockout model is applied [33,34]. To date there is no significant evidence to identify the dominant mechanism in the ^{6}Li(n,t) reaction as pickup or knockout. Unlike the pickup model, the knockout model has been scarcely applied to the ^{6}Li(n,t) reaction so far. Furthermore, some successful applications of the knockout model for the light nuclear reactions have been reported [34–37]. Consequently, it is essential to investigate the availability of the knockout model for the ^{6}Li(n,t) reaction.

The ground state of ^{6}Li is dominated by two overlapping configurations: $t + ^3$He and $d + \alpha$ [38]. Under these two-cluster assumptions of the target nucleus, there are two reaction processes in the knockout model, namely, the knockout process and the heavy-particle knockout process [35,39]. In the knockout process for the ^{6}Li(n,t) reaction, the incident neutron knocks out a triton from the target, so the effective interaction is between the neutron and the triton. In the heavy-particle knockout process for the ^{6}Li(n,t) reaction, the α particle in the target nucleus ^{6}Li is supposed to be emitted from the ground state, and the incident neutron is captured by the deuteron to form the residual triton. The effective interaction is, thus, between the incident neutron and the α particle. In addition to the knockout process, the heavy-particle knockout process based on DWBA or plane-wave Born approximation is also very important to explain the experimental data of the differential cross sections [20,35,39–42]. In conclusion, based on the two-cluster assumption that ^{6}Li consists of $t + ^3$He or $d + \alpha$, the knockout process and heavy-particle knockout process are both considered in our DWBA calculation in the energy range from 1.0 eV to 3.0 MeV.

Due to the effects of the discrete excited energy levels of the compound nucleus, the reaction cross sections with resonance structures cannot be reproduced by the direct nuclear reaction model. In this paper, an effective excited energy formula is proposed to consider the contributions from the energy levels of the compound nucleus. Four optimal parameters contained in this formula are all obtained by the simulated annealing algorithm [43].

The shapes of the measured differential cross sections, presenting 90° approximate symmetry in the incident energy range from 0.1 to 1.0 MeV, indicate that the contribution of the compound nuclear reaction cannot be ignored in this energy region. The Hauser-Feshbach model with width fluctuation correction is a general and basic tool used for the analysis of the compound nuclear reactions. However, the cross sections with resonance peaks can hardly be adequately calculated with the Hauser-Feshbach model since the statistical hypothesis is not held in this energy region. Therefore, a tentative method is used to analyze the experimental angular distributions without considering its absolute cross sections in the energy range from 0.1 to 1.0 MeV. The contributions from the knockout process, heavy-particle knock-out process, and Hauser-Feshbach model are considered by this method for the calculations of the angular distributions in the energy range from 0.1 to 1.0 MeV.

In this paper, the knockout process and heavy-particle knockout process based on zero-range DWBA theory are considered in the analysis of the ^{6}Li(n,t) reaction in the energy range from 1.0 eV to 3.0 MeV. The Weierstrass

formula [44] is employed to accurately calculate the Coulomb phase shift. An effective excited energy formula is proposed to describe the effects of energy levels of the compound nucleus. In addition, the Hauser-Feshbach model is used to improve the calculated results in the energy range from 0.1 to 1.0 MeV. The model calculations of the differential cross sections and angle-integrated cross sections of the emitted triton for neutron-induced ^{6}Li reaction in the energy range from 1.0 eV to 3.0 MeV are performed to reproduce the recent experimental data [9]. The calculated results are also compared with other available experimental data and the evaluated data from ENDF/B-VIII.0 and JEFF-3.3

In Sec. II, the framework of theoretical models is introduced. The comparisons of the calculated results with the experimental data and evaluated data are given in Sec. III. The summary and conclusion are given in Sec. IV.

II. THEORETICAL MODELS

A. Knockout model

For the knockout model, this is visualized as a process in which the target A consists of a "core" C and an emitted particle b, $A = C + b$, whereas the residual nucleus B is composed of a core C and an incident particle a, $B = C + a$. The conventional DWBA theory in the zero-range approximation has been developed to calculate the differential cross sections and angle-integrated cross sections of the knockout model. Angular momentum coupling and parity effects are considered in the formulas, so their conservations are held. In this paper, the knockout model is used to describe the knockout process and heavy-particle knockout process. For illustrating the physical picture, the fundamental formulas are simply given in this subsection. The detailed description can be found in Refs. [45–47].

To conveniently describe the formulas of the differential cross section and angle-integrated cross section for the $A(a, b)B$ reaction, some quantities are defined as follows:

A, B, a, b, and C are the nucleon numbers of the target nucleus, residual nucleus, incident particle, emitted particle, and core, respectively.

k_a and k_b are the wave numbers of the incident particle and emitted particle, respectively.

E_L is the kinetic energy of the incident particle in laboratory system (LS).

E_a and E_b are the kinetic energies of the incident particle and emitted particle in the center-of-mass system (CMS), respectively.

M_a, M_b, M_A, and M_B are the masses of the incident particle, emitted particle, target nucleus, and residual nucleus, respectively.

$\alpha(k)$ is the spectroscopic factor.

G_0 is the strength of a zero-range interaction.

U_k is the excited energy of the residual nucleus.

L_a, I_a, and J_a are the orbital, spin, and total angular momentum of the incident particle, respectively.

L_b, I_b, and J_b are the orbital, spin, and total angular momentum of the emitted particle, respectively.

l is the transfer angle momentum.

I_A and I_B are the spins of the target nucleus and residual nucleus, respectively.

I_C is the spin of the core.

The angular momentum coupling relations are given below,

$J_a = I_a + L_a$,

$J_b = I_b + L_b$,

$l = L_a - L_b$,

$J_{BA} = I_B - I_A$,

$J_{ba} = I_b - I_a$.

According to the conservation of angular momentum,

$I_a + L_a + I_A = I_b + L_b + I_B$.

J_{BA} and l can be written as

$J_{BA} = J_a - J_b$,

$l = J_{BA} + J_{ba}$.

π_A and π_B are the parities of the target nucleus and residual nucleus, respectively.

The conservation of parity, $\delta[\pi_A\pi_B, (-1)^l]$.

The differential cross section can be expressed as

$$\frac{d\sigma_{ab}(E_a, E_b, \theta)}{d\Omega} = \frac{k_b}{k_a}\frac{10}{(2I_A+1)(2I_a+1)} \times\alpha(k)G_0^2\sum_{J_{BA}}\sigma_{J_{BA}}(\theta), \tag{1}$$

where $\sigma_{J_{BA}}(\theta)$ can be expressed as

$$\sigma_{J_{BA}}(\theta) = \sum_{m_{J_{BA}}m_b m_a}\left|\sum_{J_{ba}L_aJ_aL_bJ_bl}\delta[\pi_A\pi_{B(k)}, (-1)^l](-1)^{J_{BA}-J_a-J_b}\hat{J}_{ba}\hat{L}_a\hat{J}_b\langle L_a, 0, I_a, m_a|J_a, m_a\rangle \times\langle L_b, -m_{J_{BA}}, I_b, m_b \mid J_b, -m_{J_{BA}}+m_b\rangle\langle J_b, m_b-m_{J_{BA}}, J_{BA}, m_{J_{BA}}-m_b+m_a|J_a, m_a\rangle \times\begin{Bmatrix} J_a & I_a & L_a \\ J_b & I_b & L_b \\ J_{BA} & J_{ba} & l\end{Bmatrix}X^{L_bJ_bL_aJ_a}_{lJ_{ba}J_{BA}}(-1)^{m_{J_{BA}}}\left[\frac{(2L_b+1)(L_b-m_{J_{BA}})!}{4\pi(L_b+m_{J_{BA}})!}\right]^{1/2}P^{m_{J_{BA}}}_{L_b}(\theta)\right|, \tag{2}$$

where $m_{J_{BA}}$, m_a, and m_b are the magnetic quantum numbers of J_{BA}, I_a, and I_b, respectively. $P^{m_{J_{BA}}}_{L_b}(\theta)$ are the Legendre polynomials. $X^{L_bJ_bL_aJ_a}_{lJ_{ba}J_{BA}}$ can be written as

$$X^{L_bJ_bL_aJ_a}_{lJ_{ba}J_{BA}} = \frac{1}{\sqrt{E_aE_b}}\hat{L}_a\hat{L}_b i^{L_a+L_b-l}\langle L_b, 0, L_a, 0|l, 0\rangle\frac{B}{A}\int dr_a\chi^{J_b}_{L_b}\left(k_b, \frac{A}{B}r_a\right)\chi^{J_a}_{L_a}(k_a, r_a)F^{ZR}_{lJ_{ba}J_{BA}}(r_a), \tag{3}$$

where $\chi^{J_a}_{L_a}(k_a, r_a)$ and $\chi^{J_b}_{L_b}(k_b, \frac{A}{B}r_a)$ are the distorted-wave functions of the incident channel and the ejected channel, respectively, which are calculated by the optical model. $F^{ZR}_{lJ_{ba}J_{BA}}(r_a)$ can be written as

$$F^{ZR}_{lJ_{ba}J_{BA}}(r_a) = \frac{1}{\sqrt{4\pi}} i^{l-l_\alpha+l_\beta}(-1)^{I_A-I_C+j_\beta+2I_b+2I_a}\hat{I}_A\hat{I}_B\hat{l}_\alpha\hat{j}_\alpha\hat{l}_\beta\hat{j}_\beta\hat{J}_{BA}\hat{J}_{ba}\langle l_\alpha, 0, l_\beta, 0|l, 0\rangle$$
$$\times W(j_\alpha, I_B, j_\beta, I_A; I_C, J_{BA})\left(\frac{A}{C}\right)^3 U_{n_\alpha l_\alpha j_\alpha}\left(\frac{A}{C}r_a\right)U_{n_\beta l_\beta j_\beta}\left(\frac{A}{C}r_a\right)\begin{Bmatrix} j_\alpha & I_a & l_\alpha \\ j_\beta & I_b & l_\beta \\ J_{BA} & J_{ba} & l \end{Bmatrix}, \quad (4)$$

where $U_{n_\alpha l_\alpha j_\alpha}(\frac{A}{C}r_a)$ and $U_{n_\beta l_\beta j_\beta}(\frac{A}{C}r_a)$ are the wave functions of the target nucleus and residual nucleus, respectively. n_α, l_α, and j_α are the radial quantum number, orbital angular momentum, and total angular momentum of the emitted particle in the target nucleus; n_β, l_β, and j_β are the radial quantum number, orbital angular momentum, and total angular momentum of the incident particle in the residual nucleus.

The definition $\hat{j} \equiv \sqrt{2j+1}$ is used in the above equations.

The angle-integrated cross section can be expressed as

$$\sigma_{ab}(E_a, E_b) = \alpha(k)G_0^2\frac{k_b}{k_a}\frac{10}{(2I_A+1)(2I_a+1)}$$
$$\times 2\pi\sum_{J_{BA}}\int_0^{180}\sigma_{J_{BA}}(\theta)\sin\theta\, d\theta. \quad (5)$$

B. Effective excited energy

Due to the influences of the discrete excited energy levels of the compound nucleus, it is difficult to reproduce resonance structures by the direct reaction model. Therefore, the energy levels of the compound nucleus ^{7}Li are systematically investigated, and an effective excited energy formula is proposed to describe their effects.

Considering the energy-momentum conservation in the CMS, the total energies of the incident channel and emitted channel can be expressed as

$$E^* = \frac{M_A}{M_C}E_L + B_n, \quad (6)$$

$$E^* = \frac{M_C}{M_B}\varepsilon_t + B_t + U_k, \quad (7)$$

where B_n and B_t are the binding energies of the incident neutron and emitted triton in the compound nucleus, respectively. E^* is the total energy of the compound system. E_L and ε_t are the energies of the incident neutron and emitted triton, respectively. U_k is the excited energy of the residual nucleus, and U_k is 0 in our calculations. M_A, M_B, and M_C are the masses of the target nucleus, residual nucleus, and compound nucleus, respectively.

Considering the conservation of energy between the incident channel and the emitted channel, one can get Eq. (8),

$$\frac{M_A}{M_C}E_L + B_n = \frac{M_C}{M_B}\varepsilon_t + B_t. \quad (8)$$

Equation (8) can be further simplified as

$$\varepsilon_t = \frac{M_B}{M_C}\left[\frac{M_A}{M_C}E_L + (B_n - B_t)\right]$$

or

$$E_L = \frac{M_C}{M_A}\left(\frac{M_C}{M_B}\varepsilon_t + B_t - B_n\right). \quad (9)$$

To consider the energy levels of the compound nucleus ^{7}Li, a part of E^*, labeled as $E_C(k)$, is assumed to contribute to the energy levels of the compound nucleus rather than triton emission. However, the residual part of E^*, labeled as $E^*_{\rm eff}$, totally contributes to the triton emission. Therefore, E^* can be written as

$$E^* = E_C(k) + E^*_{\rm eff}, \quad (10)$$

where $E^*_{\rm eff}$ is named as the effective excited energy.

According to Eq. (7), the relationship between the effective excited energy and the effective triton emitted energy ε'_t can be written as

$$E^*_{\rm eff} = \frac{M_C}{M_B}\varepsilon'_t + B_t. \quad (11)$$

Inserting Eqs. (7) and (10) into Eq. (11), one can get Eq. (12),

$$\varepsilon'_t = \varepsilon_t - \frac{M_B}{M_C}E_C(k). \quad (12)$$

Considering the conservation of energy between the incident channel and the emitted channel, one can get Eq. (13),

$$\frac{M_A}{M_C}E'_L + B_n = \frac{M_C}{M_B}\varepsilon'_t + B_t, \quad (13)$$

where E'_L is named as effective incident energy, contributing to the direct reaction model calculation.

Inserting Eq. (12) into Eq. (13), one can get Eq. (14),

$$\frac{M_A}{M_C}E'_L + B_n = \frac{M_C}{M_B}\left[\varepsilon_t - \frac{M_B}{M_C}E_C(k)\right] + B_t, \quad (14)$$

then,

$$E'_L = \frac{M_C}{M_A}\left\{\frac{M_C}{M_B}\left[\varepsilon_t - \frac{M_B}{M_C}E_C(k)\right] + B_t - B_n\right\}$$
$$= \frac{M_C}{M_A}\left[\frac{M_C}{M_B}\varepsilon_t + (B_t - B_n) - E_C(k)\right]$$
$$= E_L - \frac{M_C}{M_A}E_C(k). \quad (15)$$

Furthermore, it is assumed that $E_C(k)$ is a function of widths and excited energies of the energy levels with an approximate Gaussian distribution form. $E_C(k)$ can be expressed as

$$E_C(k) = \sum_i A_i E_L \exp\left(-\frac{4(E^* - E_i)^2}{9\Gamma_i^2}\right), \tag{16}$$

where E_i and Γ_i are the energy and width of the ith discrete energy level of the compound nucleus, respectively. A_i is adjustable parameter.

According to our assumption Eq. (16), the expected value of energy distribution is dependent on E_i. The standard deviation of energy distribution is determined by the energy level width Γ_i. A low Γ_i indicates that the energy of the energy level tends to be close to the maximum value, whereas a high Γ_i indicates that the energy of the energy level is spread out over a wide range.

The binding energy of the incident neutron in the compound nucleus ^{7}Li is 7.25 MeV, whereas the energies of the first three energy levels of ^{7}Li are less than 7 MeV. Moreover, according to the calculations, the postseven energy levels have no contribution to the cross sections for the ^{6}Li(n, t) reaction in incident neutron energy below 3.0 MeV. So only fourth–seventh energy levels are adopted in the calculation.

The energy E_i ($i = 4$–7) and width Γ_i ($i = 4$–7) of the discrete energy levels of the compound nucleus are derived from the experimental measurements [48–50] as fixed input parameters. A_i ($i = 4$–7) are treated as adjustable parameters determined by fitting the experimental data.

In terms of Eq. (16), Eq. (15) can be rewritten as

$$E'_L = E_L - \frac{M_C}{M_A}\sum_{i=4} A_i E_L \exp\left(-\frac{4(E^* - E_i)^2}{9\Gamma_i^2}\right). \tag{17}$$

Equation (17), named the effective incident energy formula, is employed in the knockout model.

C. Hauser-Feshbach model with width fluctuation correction

The general formula of the differential cross section for the Hauser-Feshbach model is given in Refs. [51,52]. For the incident particle and the outgoing particle with spins of $\frac{1}{2}$, the coefficients of the Legendre polynomials in the general formula can be reduced to a recurrence formula [53]. The differential cross section expressed by a recurrence formula in the j-j coupling scheme can be written as

$$\frac{d\sigma_{a,b}}{d\Omega} = \frac{1}{8k_a^2(2I_0+1)}\sum_{LJ\pi l j l' j'}\Big\{\delta[\pi, (-1)^l\pi_0] \times \delta[\pi, (-1)^{l'}\pi_k,]Q_L^J(I_0 I'_k j j')(2J+1) \times \frac{T_{lj}(E)T_{l'j'}(E')}{T^{J\pi}}P_L(\cos\theta)W^{J\pi}_{alj,bl'j'}\Big\}, \tag{18}$$

where l and j are the orbital angular momentum and total angular momentum of the incident particle, respectively. l' and j' are the orbital angular momentum and total angular momentum of the emitted particle, respectively. I_0 and I'_k are the spins of the target nucleus and residual nucleus, respectively. π_0 and π'_k are the parities of the target nucleus and residual nucleus, respectively. L is the transfer angle momentum. J and π are the total angular momentum and parity of the total reaction channel, respectively. k_a is the wave number of the incident particle. $P_L(\cos\theta)$ represents the Legendre polynomials. $T_{lj}(E)$, $T_{l'j'}(E')$, and $T^{J\pi}$ are the penetration coefficients of the incident channel, the outgoing channel, and the total reaction channel, respectively. $W^{J\pi}_{alj,bl'j'}$ is the width fluctuation correction factor. The recurrence formula of $Q_L^J(I_0 I'_k j j')$ can be expressed as

$$Q^J_{L+2}(I_0 I'_k j j') = \left(\frac{L+1}{L+2}\right)^2\left(\frac{2L+5}{2L+1}\right)[(2J+L+3)(2J+L+2)(2J-L-1)(2J-L)(2j+L+2) \times (2j-L)(2j'+L+2)(2j'-L)]^{-1}\omega_{L+2}(JI_0 j)\omega_{L+2}(JI'_k j')Q^J_L(I_0 I'_k j j'), \quad Q^J_0(I_0 I'_k j j') = 1. \tag{19}$$

The recurrence formula of $\omega_{L+2}(JI_0 j)$ can be expressed as

$$\omega_{L+2}(JI_0 j) = \alpha_{L+1}\alpha_L - \beta_{L+1} - \frac{\alpha_{L+1}\beta_L}{\alpha_{L-1}} - \frac{\alpha_{L+1}\beta_L\beta_{L-1}}{\alpha_{L-1}\omega_L(JI_0 j)},$$
$$\omega_2(JI_0 j) = 6\mathcal{A}(\mathcal{A}+1) - 8J(J+1)j(j+1),$$
$$\mathcal{A} = I_0(I_0+1) - J(J+1) - j(j+1). \tag{20}$$

The coefficients α_L and β_L can be written as

$$\alpha_L = \frac{2L+1}{L+1}[-2\mathcal{A} - L(L+1)],$$
$$\beta_L = \frac{L}{L+1}[(2j+1)^2 - L^2][(2J+1)^2 - L^2]. \tag{21}$$

D. Optical model

The phenomenological spherical OMP is employed in the calculations of the distorted wave functions. The OMP adopted in this paper is the Woods-Saxon type [54] for the real part, the Woods-Saxon, the derivative Woods-Saxon type for the imaginary parts corresponding to the volume and surface absorptions, respectively, and the Thomas form for the spin-orbit part.

The energy dependence of the OMP depths is expressed as follows:

The real part,

$$V_r(E_L) = V_0 + V_1 E_L + V_2 E_L^2 + V_3\frac{A-2Z}{A} + V_4\left(\frac{Z}{A^{1/3}}\right). \tag{22}$$

TABLE I. Neutron and triton parameters of the OMP obtained from Ref. [56]. Only two neutron parameters a_r and r_r are slightly adjusted in this paper.

Parameter	Neutron	Triton	Parameter	Neutron	Triton
V_0	36.8312	155.56735	U_2	−0.03566	0.13199
V_1	−0.75812	−0.17920	V_{so}	6.24281	8.90004
V_2	0.004462	−0.44748	r_r	1.546276	2.13954
V_3	−24	0.03094	r_s	1.338627	1.50830
V_4	0	6.93479	r_v	1.99	1.97878
W_0	0.323586	10.19150	r_{so}	1.526276	1.93601
W_1	1.030198	0.72566	a_r	0.670343	1.20778
W_2	−12.0	0.00021	a_s	0.340605	0.96054
U_0	−0.75004	−8.80010	a_v	0.797172	0.92900
U_1	0.75	3.24032	a_{so}	0.736343	1.62509

The imaginary part of surface absorption,

$$W_s(E_L) = \max\left\{0, W_0 + W_1 E_L + W_2 \frac{(A-2Z)}{A}\right\}. \quad (23)$$

The imaginary part of volume absorption,

$$W_v(E_L) = \max 0, U_0 + U_1 E_L + U_2 {E_L}^2 , \quad (24)$$

where Z and A are the charge number and mass number of the target nucleus or residual nucleus, respectively. E_L is the incident neutron energy in the LS. The radius of the real part, the surface absorption, the volume absorption, and the spin-orbit couple potential are r_r, r_s, r_v, and r_{so}. The diffuseness width of the real part, the surface absorption, the volume absorption, and the spin-orbit couple potential are a_r, a_s, a_v, and a_{so}. The unit of the potential depth V_r, W_s, W_v, and V_{so} are in MeV; the lengths r_r, r_s, r_v, r_{so}, a_r, a_s, a_v, and a_{so} are in fermis. The unit of the energy E_L is in MeV.

E. Simulated annealing algorithm

The four parameters A_i ($i = 4$–7) in the effective excited energy formula (17) can be properly adjusted to fit the measured differential cross sections for the ^{6}Li(n,t) reaction. The simulated annealing algorithm [43], which automatically searches the global minimum or maximum of the cost function, is used to obtain a set of optimal parameters in the model calculation.

The best parameters are optimized with the usual minimization of the cost function χ^2, which represents the deviation of the calculated results from the experimental values.

The cost function χ^2 can be expressed as

$$\chi^2 = \frac{1}{N}\sum_i [\sigma_{i,\mathrm{theo}}(\theta) - \sigma_{i,\mathrm{exp}}(\theta)]^2. \quad (25)$$

TABLE II. The parameters of phenomenological formula (17) optimized with the simulated annealing algorithm.

A_4	A_5	A_6	A_7
0.2400386	0.0000345	0.7192635	0.0217633

The simulated annealing algorithm, which reportedly performed well in the presence of a high number of variables [55], is able to jump out of the local optimization and search the next point. Therefore, it is reliable to obtain optimal values of the parameters A_i ($i = 4$–7).

III. RESULTS AND ANALYSIS

The parameters of the OMP are rather critical in the DWBA calculation. The neutron and triton parameters of the OMP for the ^{6}Li(n,t) reaction were searched automatically by fitting the experimental data of total nonelastic elastic-scattering cross sections and angular distributions in the energy range from 5.0 to 20.0 MeV [56] by the APMN code [57] in our previous works. The extrapolation had been successfully applied to determine the parameters of the OMP at low energies in the previous DWBA calculations of the light nucleus reaction [25,30]. Therefore, the parameters of the OMP for the ^{6}Li(n,t) reaction in the energy range from 5.0 to 20.0 MeV [56] are extrapolated to the present DWBA calculation. Only two neutron parameters (a_r and r_r) of the

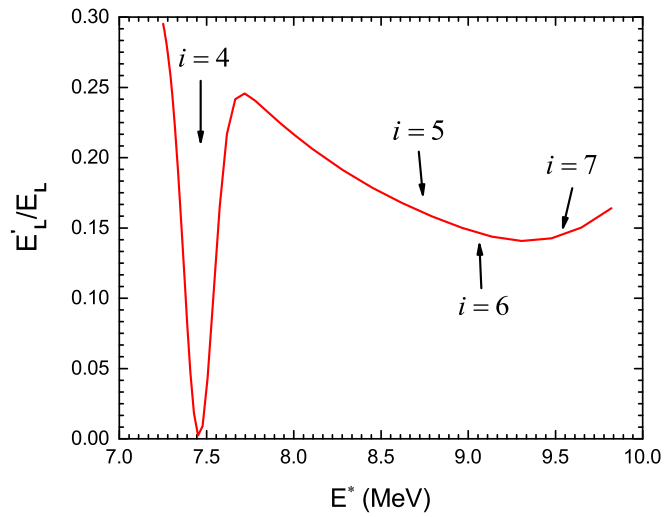

FIG. 1. The excited energy dependence of Eq. (26) for the ^{6}Li(n,t) reaction below 3 MeV. The positions of the fourth–seventh energy levels of the compound nucleus are shown in this figure.

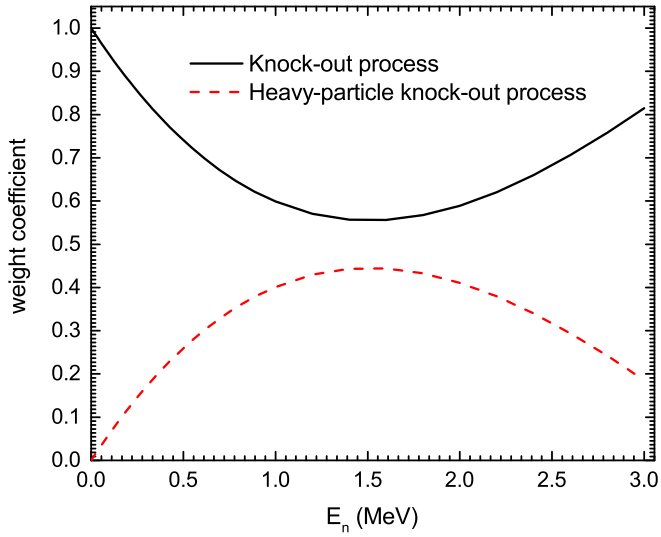

FIG. 2. The incident energy dependence of the weighting coefficients for the knockout process and the heavy-particle knockout process in the energy range from 1 eV to 3 MeV.

OMP are slightly adjusted from 0.736 343 and 1.526 276 to 0.670 343 and 1.546 276, respectively. The neutron and triton parameters of the OMP used in this paper are given in Table I.

Based on the 1200 measured differential cross sections of 80 energy points from 1.0 eV to 3.0 MeV [9], the minimal deviation between the experimental data and the model calculation is searched by the simulated annealing algorithm. In Table II for the optimal parameters of the effective excited energy formula (17), the values of A_4 and A_6 are obviously much larger than those of A_5 and A_7. It implies that the effects from the fourth and sixth energy levels of the compound nucleus on cross sections are larger than those of others. It is reasonable because there is an obvious resonance peak at around 0.24 MeV in the measured angle-integrated cross

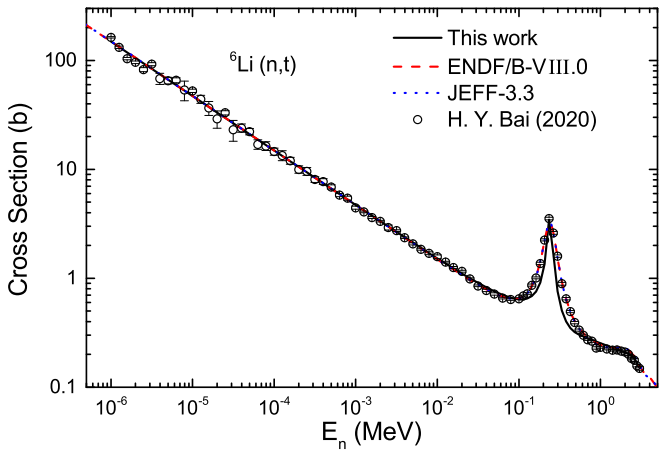

FIG. 3. Comparison of the calculated angle-integrated cross sections of the emitted triton for the neutron-induced ^{6}Li reaction with the experimental data [9] and the evaluated data from ENDF/B-VIII.0 and JEFF-3.3.

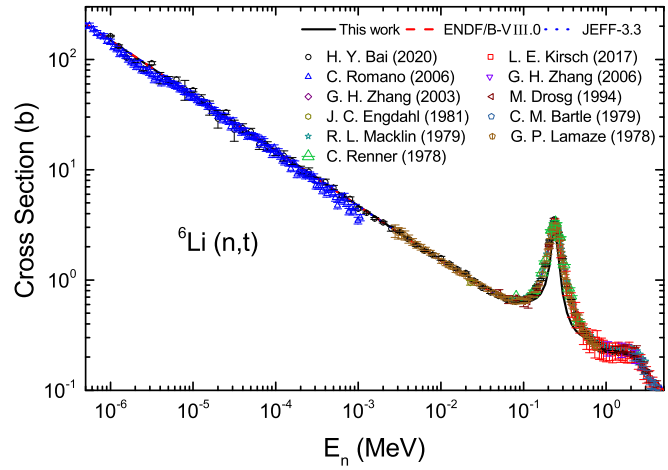

FIG. 5. The same as Fig. 3 but for different experimental data [9,79–88] as labeled in this figure.

sections due to the fourth energy level of the compound nucleus. Because of the large energy width of the sixth energy level ($\Gamma_6 = 2.752$ MeV), there is no obvious resonance peak caused by the sixth energy level in the angle-integrated cross sections.

According to Eq. (17), the ratio of the effective incident energy to the actual incident energy can be written as

$$\frac{E'_L}{E_L} = 1 - \frac{M_C}{M_A}\sum_{i=4} A_i \exp\left(-\frac{4(E^* - E_i)^2}{9\Gamma_i^2}\right). \tag{26}$$

The excited energy E^* dependence of the ratio for the ^{6}Li(n,t) reaction in the incident energy range from 1.0 eV to 3.0 MeV is shown in Fig. 1. It can be seen that the effects of the energy levels of the compound nucleus cover the whole excited energy region, and the effective incident energy is less than one-third of the actual incident energy in this region. Obviously, the ratio reaches its minimum value at 7.454 MeV corresponding to the fourth energy level of the compound nucleus.

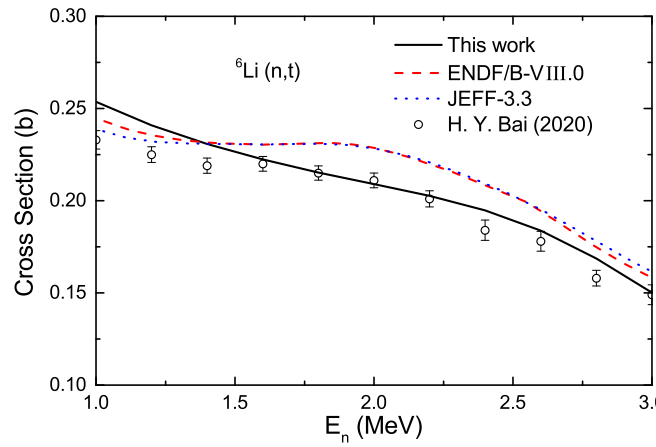

FIG. 4. The same as Fig. 3 but incident energy only in 1.0–3.0 MeV.

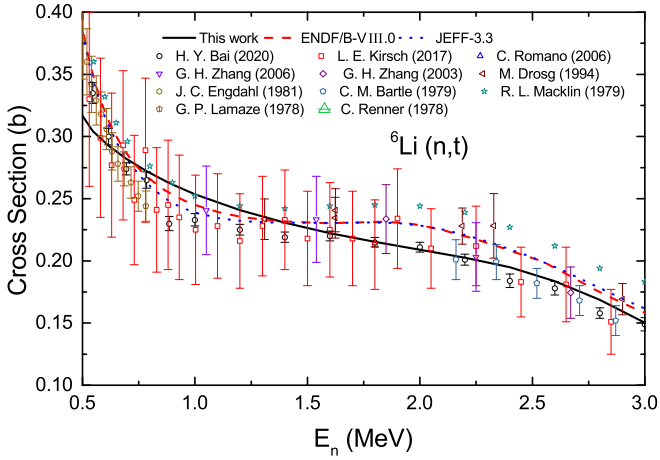

FIG. 6. The same as Fig. 3 but incident energy only in 0.5–3.0 MeV for different experimental data [9,79–88] as labeled in this figure.

The spectroscopic factor is related to the preformation probability of a cluster configuration in a nucleus [58]. For the configuration of $t + ^3$He in ^{6}Li, the spectroscopic factors can be found in Refs. [38,59–64]. The results are between values of 0.1 and 0.9. Similarly, the published spectroscopic factors for the configuration of $d + \alpha$ vary from 0.42 to 1.39 [59,65–78]. Obviously, the spectroscopic factors extracted from the different reaction types at different energies fail to agree with each other. Due to lack of self-consistent research on the spectroscopic factors for configurations of $t + ^3$He and $d + \alpha$, the spectroscopic factors of the knockout process and heavy-particle knockout process are assumed to be 1.0 in this paper.

In order to illustrate the relative contributions from these two different reaction processes, the different values of the

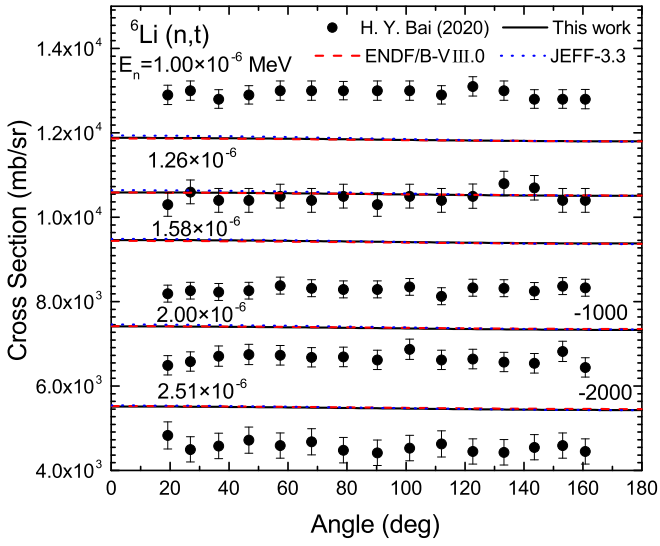

FIG. 7. Comparisons of the calculated differential cross sections of the emitted triton for the neutron-induced ^{6}Li reaction with the experimental data [9] and the evaluated data from ENDF/B-VIII.0 and JEFF-3.3.

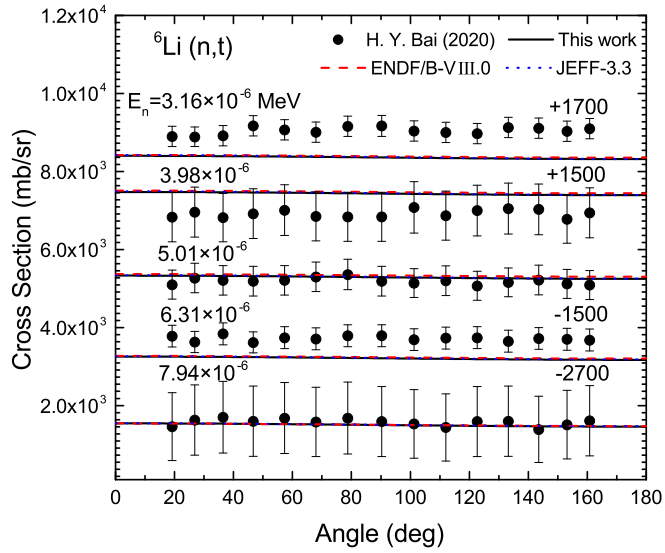

FIG. 8. The same as Fig. 7 but for different incident energies as labeled in this figure.

weighting coefficients for the knockout process and heavy-particle knockout process are used in this paper. The energy dependence of the weighting coefficients is particularly noticeable. In other words, the relative contributions from these two processes are energy dependent. Furthermore, the calculated results can precisely reproduce the experimental data at most of the energy points if the weighting coefficients represent a cubic function of energy. The relationship between the weighting coefficients and the incident energy for the knockout process can be, thus, expressed as

$$P_{\text{knockout}} = 1.0 - 0.64934E_L + 0.27411E_L^2 - 0.02608E_L^3, \quad E_L \leqslant 3 \text{ MeV}. \tag{27}$$

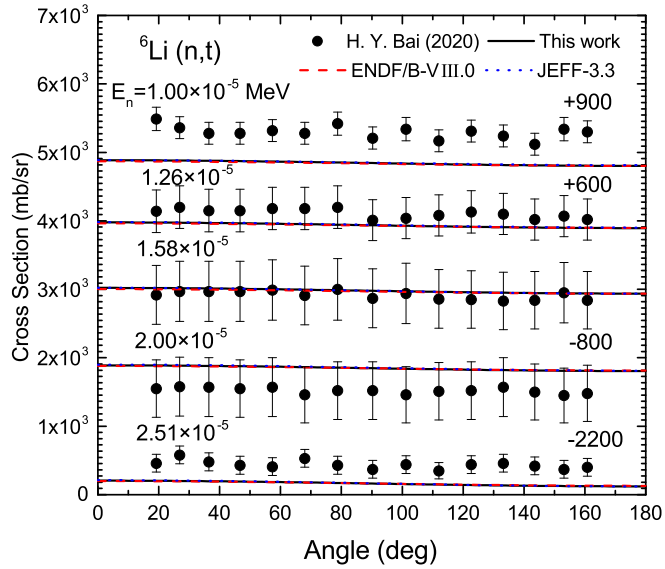

FIG. 9. The same as Fig. 7 but for different incident energies as labeled in this figure.

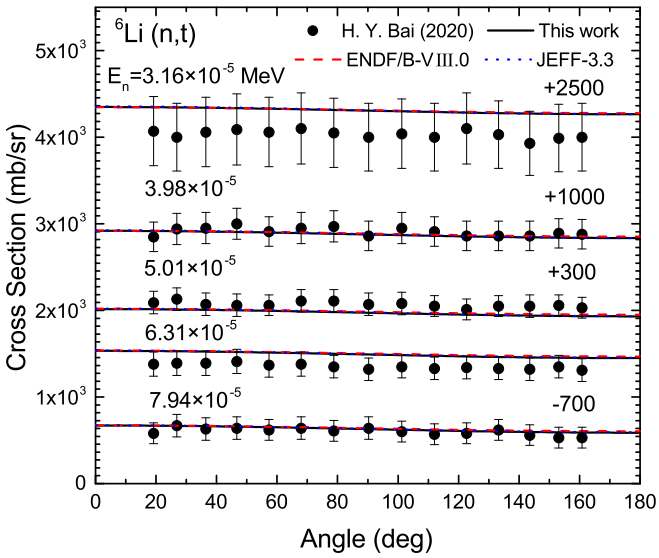

FIG. 10. The same as Fig. 7 but for different incident energies as labeled in this figure.

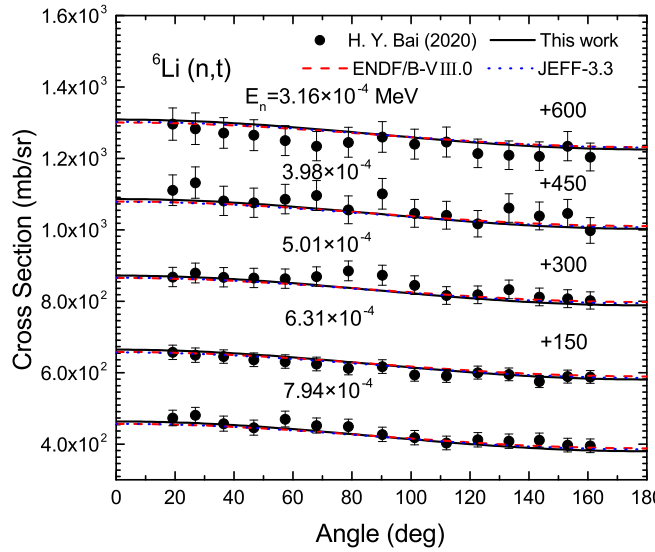

FIG. 12. The same as Fig. 7 but for different incident energies as labeled in this figure.

The weighting coefficients for the heavy-particle knockout process are $(1 - P_{\text{knockout}})$. The incident energy dependence of the weighting coefficients in the energy range from 1.0 eV to 3.0 MeV is shown in Fig. 2.

The comparisons of the calculated results with the measurements of the differential cross sections and angle-integrated cross sections for the ^{6}Li(n, t) reaction in the incident neutron energy range from 1.0 eV to 3.0 MeV was performed.

The comparisons of the calculated angle-integrated cross sections with the recently measured data [9] and the evaluated data from ENDF/B-VIII.0 and JEFF-3.3 for the ^{6}Li(n, t) reaction are shown in Figs. 3 and 4. In Fig. 3, the calculated results below 0.1 MeV agree well with the measurement except in the energy range from 1 to 100 eV due to the fluctuation of neutron energy spectrum for experimental measurement in this region [9]. The shape of experimental data above 0.1 MeV can be reasonably reproduced by the calculated results, whereas the calculations are slightly worse in the energy range from 0.1 to 0.6 MeV. In Fig. 4, the evaluations are obviously higher than our calculations as well as the experimental data in the energy range from 1.0 to 3.0 MeV.

Previous measurements can be used as a consistency check of the new measurement. So the available experimental data of the angle-integrated cross sections for the ^{6}Li(n, t) reaction after 1977 [9,79–88] are given in Figs. 5 and 6. It can be seen that the calculated cross sections are in agreement with most of the experimental data.

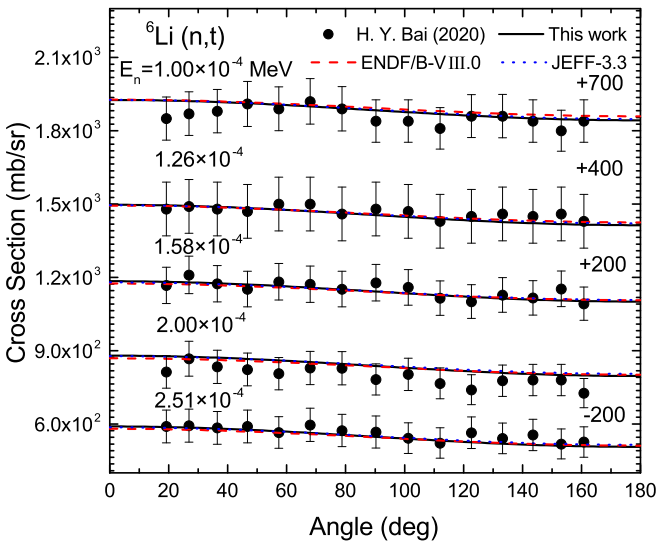

FIG. 11. The same as Fig. 7 but for different incident energies as labeled in this figure.

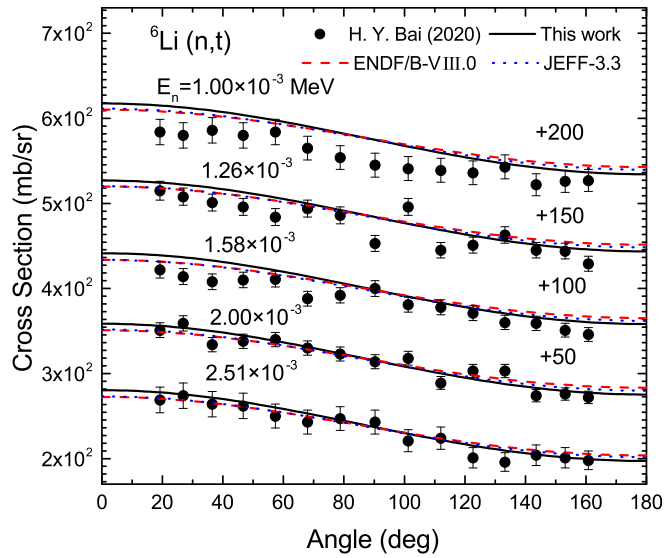

FIG. 13. The same as Fig. 7 but for different incident energies as labeled in this figure.

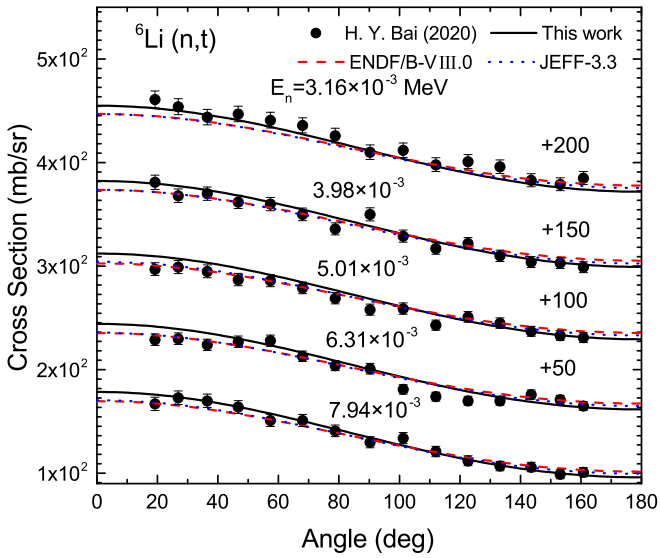

FIG. 14. The same as Fig. 7 but for different incident energies as labeled in this figure.

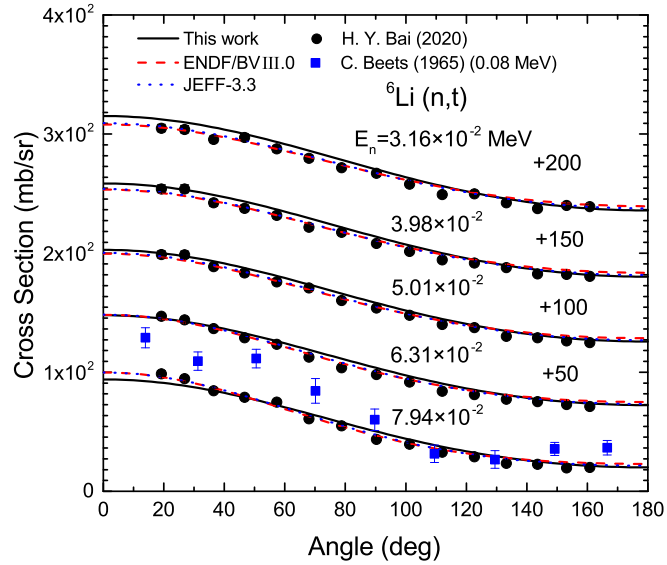

FIG. 16. The same as Fig. 7 but for different incident energies and different experimental data [9,90] as labeled in this figure.

The comparisons of the calculated differential cross sections with the available experimental data [2,9,81,82,84,85,89–99] and the evaluated data from ENDF/B-VIII.0 and JEFF-3.3 for the ^{6}Li(n,t) reaction are shown in Figs. 7–24. It can be seen that the calculated results agree very well with the measurements and the evaluations below 0.1 MeV except some discrepancies in the energy range from 1 to 100 eV due to the fluctuation of the neutron energy spectrum for experimental measurement as illuminated in Ref. [9]. The reason of the discrepancies between the calculated results and the experimental data in the energy range from 0.1 to 1.0 MeV is probably that the equilibrium reaction mechanism was not taken into consideration. The calculated results above 1.0 MeV are reasonable in accordance with the experimental data and the evaluated data except for small angles at some energy points above 2.0 MeV. The discrepancies for small angles grow with the increase in incident energy. The reason could be the emergence of other reaction mechanisms, i.e., the preequilibrium mechanism [7].

It is worth mentioning that Engdahl's experimental data at 0.0228 MeV from EXFOR [8] is lower than the calculated result with two orders of magnitude, and the appropriate experimental data can be found in Ref. [84] and used in Fig. 15.

Figure 25 shows the partial differential cross sections of the emitted triton from the knockout process and heavy-particle knockout process at incident energies of 1.4, 2.4, and 3.0 MeV. The black solid lines denote the total differential cross sections of the emitted triton for the neutron-induced ^{6}Li

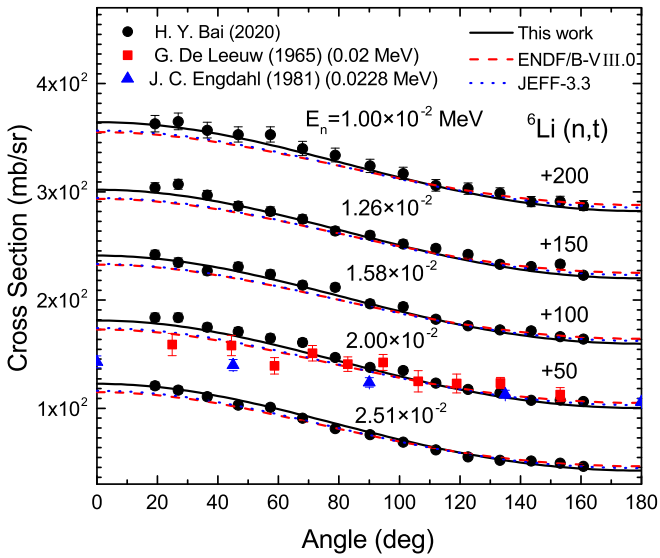

FIG. 15. The same as Fig. 7 but for different incident energies and different experimental data [9,84,89] as labeled in this figure.

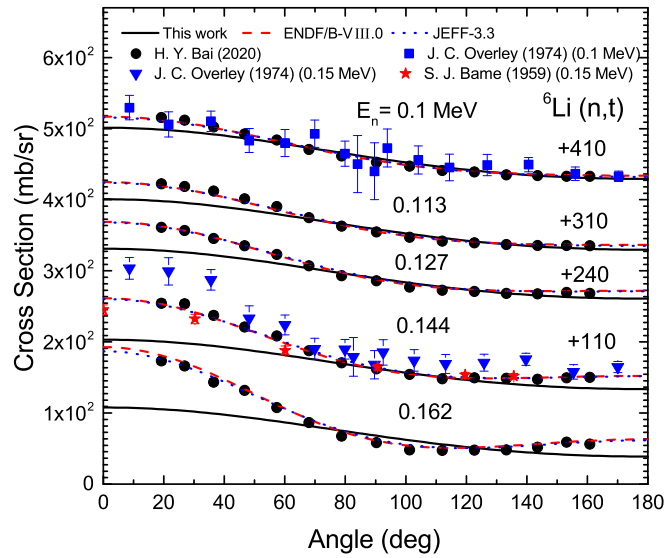

FIG. 17. The same as Fig. 7 but for different incident energies and different experimental data [9,91,92] as labeled in this figure.

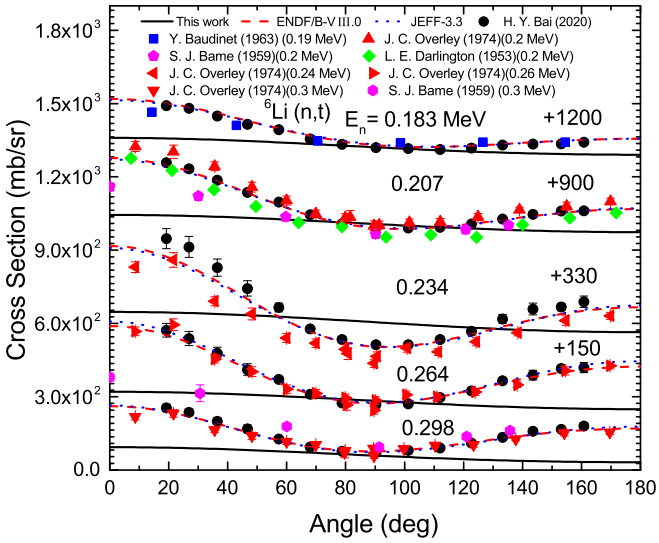

FIG. 18. The same as Fig. 7 but for different incident energies and different experimental data [9,91–94] as labeled in this figure.

reaction. The red dashed lines and blue dotted lines denote the contributions from the knockout process and heavy-particle knockout process, respectively. Obviously, the differential cross sections of the emitted triton from the knockout process have a forward trend. On the other hand, the heavy-particle knockout process is found to dominate at backward angles.

Disagreements between the calculated differential cross sections and the experimental data are mostly significant in the energy range from 0.1 and 1.0 MeV. With the increase in the incident energy, the shapes of the measured differential cross sections change from the forward trend to approximate 90° symmetry and back to the forward trend again. Furthermore, it is arduous to fit the shapes of the measured differential cross

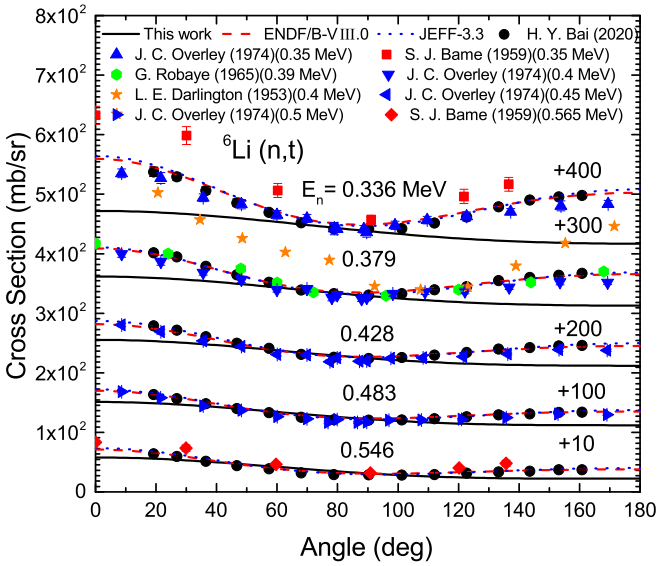

FIG. 19. The same as Fig. 7 but for different incident energies and different experimental data [9,91,92,94,95] as labeled in this figure.

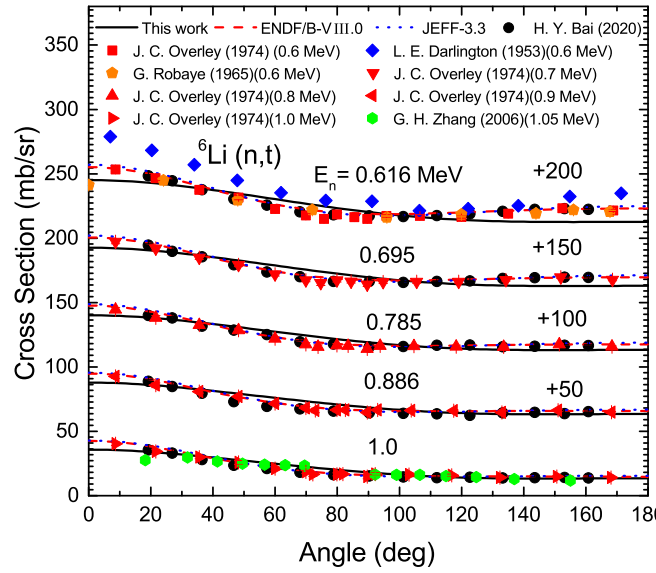

FIG. 20. The same as Fig. 7 but for different incident energies and different experimental data [9,81,91,94,95] as labeled in this figure.

sections in the energy range from 0.1 to 1.0 MeV by means of the knockout process and heavy-particle knockout process. The features displayed by the measured differential cross sections suggest that the equilibrium reaction is very important in this energy region. The Hauser-Feshbach model is a general and basic tool used in the analysis of the equilibrium reaction. However, due to the statistical hypothesis inapplicable to this energy region, the cross sections with the resonance peak can hardly be adequately calculated by the Hauser-Feshbach model, which fails to reproduce the measured angle-integrated cross sections for the ^{6}Li(n,t) reaction below 3.0 MeV. In order to investigate the effect of the equilibrium reaction

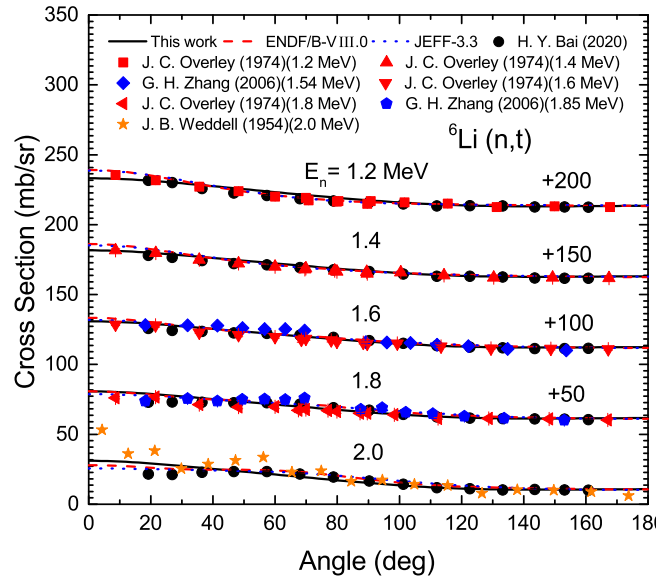

FIG. 21. The same as Fig. 7 but for different incident energies and different experimental data [9,81,91,96] as labeled in this figure.

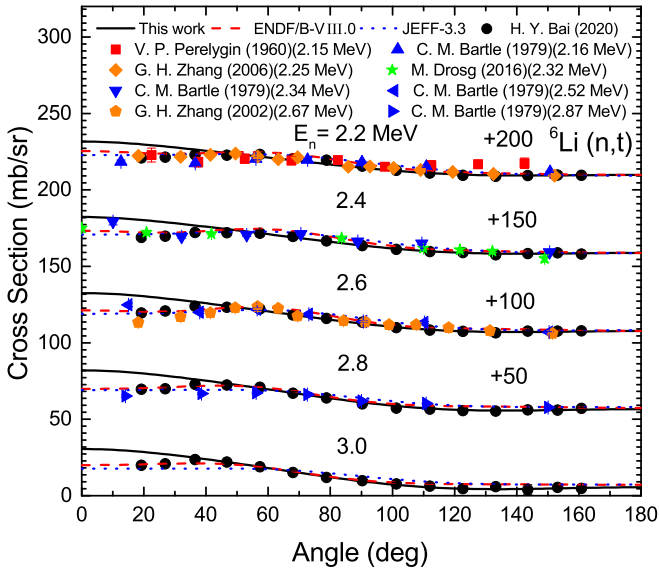

FIG. 22. The same as Fig. 7 but for different incident energies and different experimental data [9,81,82,85,97,98] as labeled in this figure.

mechanism, a tentative method is used to analyze the shapes of the measured angular distributions without considering its absolute cross sections in the energy range from 0.1 to 1.0 MeV. First of all, the absolute differential cross sections in ENDF-6 formats can be represented as a Legendre polynomial series [100],

$$\frac{d\sigma}{d\Omega} = \frac{\sigma_s(E_L)}{2\pi} \sum_{l=0} \frac{2l+1}{2} f_l P_l(\cos\theta), \tag{28}$$

where $\sigma_s(E_L)$ is the angle-integrated cross section at E_L MeV. And f_l represents the coefficients of the Legendre polynomials. The absolute differential cross sections calculated with

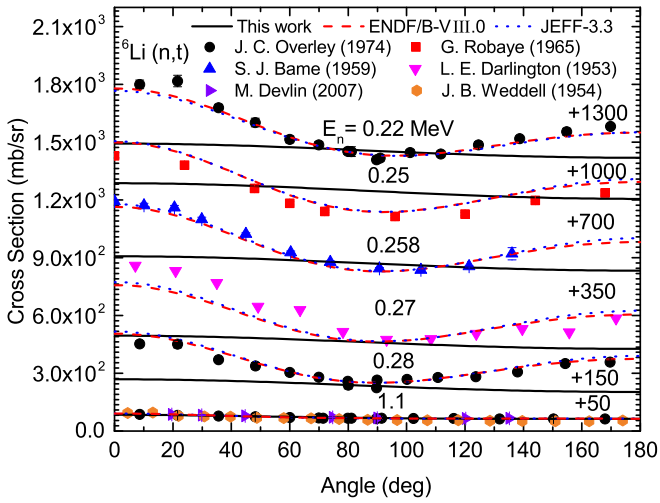

FIG. 23. The same as Fig. 7 but for different incident energies and different experimental data [2,91,92,94–96] as labeled in this figure.

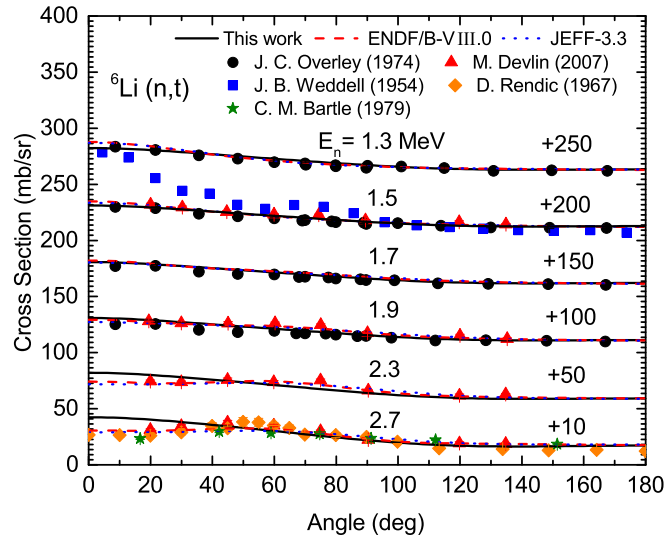

FIG. 24. The same as Fig. 7 but for different incident energies and different experimental data [2,85,91,96,99] as labeled in this figure.

different reaction mechanisms can also be expressed as

$$\frac{d\sigma^i}{d\Omega} = \frac{\sigma_s^i(E_L)}{2\pi} \sum_{l=0} \frac{2l+1}{2} f_l^i P_l(\cos\theta), \tag{29}$$

where i represents the type of reaction mechanism.

It is assumed that only the direct reaction mechanism and the equilibrium reaction mechanism contribute to total differential cross sections in the energy range from 0.1 to 1.0 MeV. The knockout process and heavy-particle knockout process are both considered in the direct reaction mechanism.

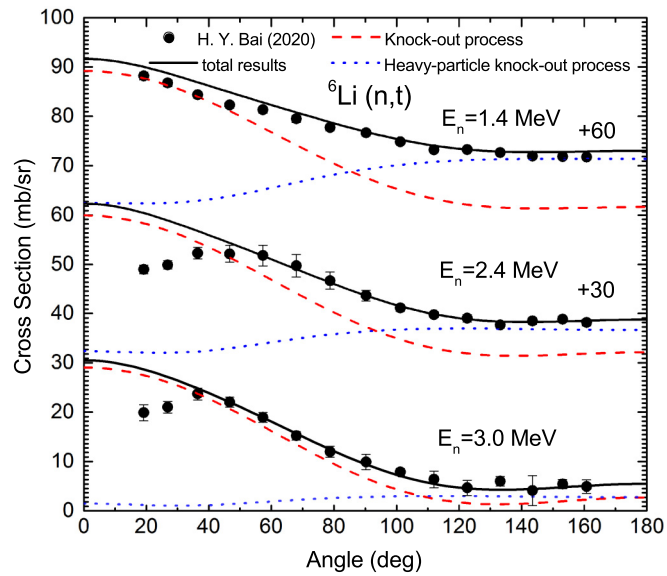

FIG. 25. The partial differential cross sections of the emitted triton for the neutron-induced ^{6}Li reaction from the knockout process and heavy-particle knockout process at incident energies of 1.4, 2.4, and 3.0 MeV.

TABLE III. The weighting coefficients $\frac{\sigma_s^{\rm equ}(E_L)}{\sigma_s^{\rm total}(E_L)}$ of the equilibrium reaction in the incident energy range from 0.1 to 1.0 MeV.

E_n (MeV)	0.1	0.113	0.127	0.144	0.162	0.183	0.207	0.234	0.264	0.298
$\frac{\sigma_s^{\rm equ}(E)}{\sigma_s^{\rm total}(E)}$	0.0	0.04	0.05	0.06	0.2	0.4	0.55	1.0	1.0	1.0
E_n (MeV)	0.336	0.379	0.428	0.483	0.546	0.616	0.695	0.785	0.886	1.0
$\frac{\sigma_s^{\rm equ}(E)}{\sigma_s^{\rm total}(E)}$	1.0	1.0	0.9	0.8	0.77	0.7	0.45	0.42	0.4	0.35

Obviously, the total differential cross sections are equal to the sum of the partial differential cross sections caused by different reaction mechanisms,

$$\frac{d\sigma^{\rm total}}{d\Omega} = \frac{d\sigma^{\rm dir}}{d\Omega} + \frac{d\sigma^{\rm equ}}{d\Omega}. \tag{30}$$

With the insertion of Eq. (29) into Eq. (30), based on the orthogonality and completeness of the Legendre polynomials, the relationship between the coefficients of the Legendre polynomials for different reaction mechanisms can be expressed as

$$f_l^{\rm total} = \frac{\sigma_s^{\rm dir}(E_L)}{\sigma_s^{\rm total}(E_L)} f_l^{\rm dir} + \frac{\sigma_s^{\rm equ}(E_L)}{\sigma_s^{\rm total}(E_L)} f_l^{\rm equ}, \tag{31}$$

where $\frac{\sigma_s^{\rm dir}(E_L)}{\sigma_s^{\rm total}(E_L)}$ and $\frac{\sigma_s^{\rm equ}(E_L)}{\sigma_s^{\rm total}(E_L)}$ are weighting coefficients of the direct reaction mechanism and equilibrium reaction mechanism, respectively. The $\frac{\sigma_s^{\rm equ}(E_L)}{\sigma_s^{\rm total}(E_L)}$'s are treated as parameters to represent the contribution from the equilibrium reaction mechanism. Obviously, the $\frac{\sigma_s^{\rm dir}(E_L)}{\sigma_s^{\rm total}(E_L)}$'s are equal to $(1 - \frac{\sigma_s^{\rm equ}(E_L)}{\sigma_s^{\rm total}(E_L)})$.

According to the discussions mentioned above, Eqs. (29) and (31) can be used to analyze the measured angular distributions. By inserting Eq. (31) into Eq. (29), one can get Eq. (32),

$$\frac{d\sigma^{\rm total}}{d\Omega} = \frac{\sigma_s^{\rm total}(E_L)}{2\pi} \sum_{l=0} \frac{2l+1}{2} P_l(\cos\theta) \times \left[\left(1 - \frac{\sigma_s^{\rm equ}(E_L)}{\sigma_s^{\rm total}(E_L)} \right) f_l^{\rm dir} + \frac{\sigma_s^{\rm equ}(E_L)}{\sigma_s^{\rm total}(E_L)} f_l^{\rm equ} \right]. \tag{32}$$

The $\sigma_s^{\rm total}(E_L)$'s are treated as fixed input parameters taken from the measured angle-integrated cross sections. The parameters $\frac{\sigma_s^{\rm equ}(E_L)}{\sigma_s^{\rm total}(E_L)}$ are determined by fitting the experimental angular distributions.

By fitting the recent experimental data [9] in the energy range from 0.1 to 1.0 MeV, the parameters $\frac{\sigma_s^{\rm equ}(E_L)}{\sigma_s^{\rm total}(E_L)}$ are listed in Table III.

As can be seen, the contribution from the equilibrium reaction mechanism is much important in this energy region. Moreover, the weighting coefficients of the equilibrium reaction vary with the incident energy and peak at 0.234 MeV. The calculated differential cross sections from Eq. (32) are compared with the experimental data [9,81,91–95] in the energy range from 0.1 to 1.0 MeV as shown in Figs. 26–29. It can be seen that the theoretical values of the newly calculated differential cross sections increase at large angles and small angles in 0.1–1.0 MeV, compared with the results by the DWBA. And the minimum values appear at around 90°. For the en-

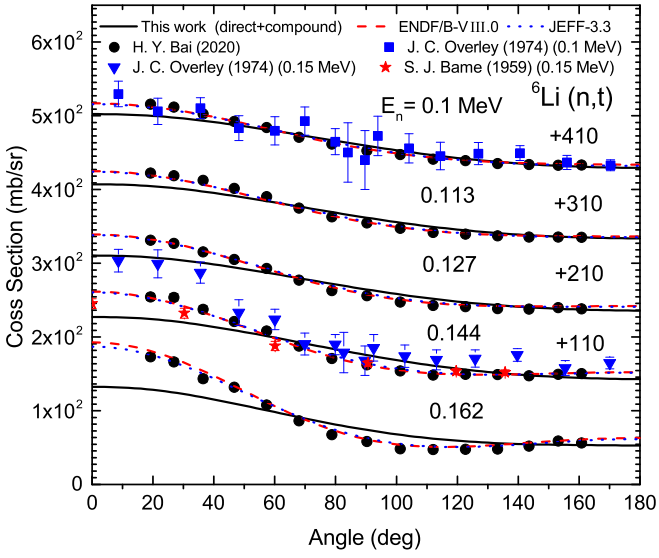

FIG. 26. The same as Fig. 7 but for different incident energies and different experimental data [9,91,92] as labeled in this figure.

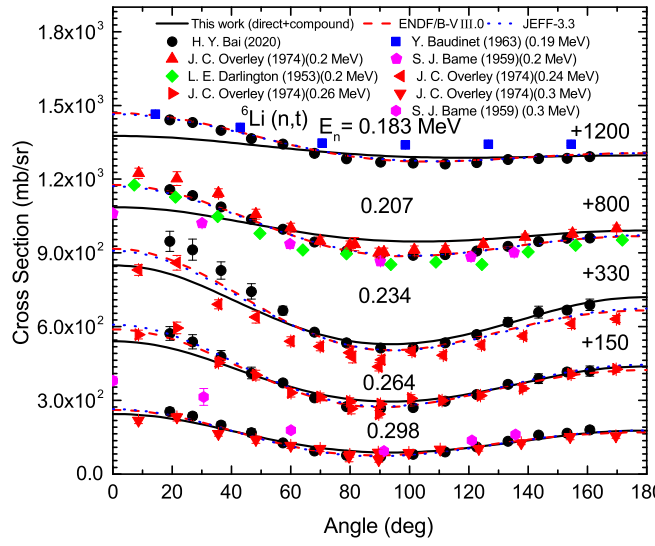

FIG. 27. The same as Fig. 7 but for different incident energies and different experimental data [9,91–94] as labeled in this figure.

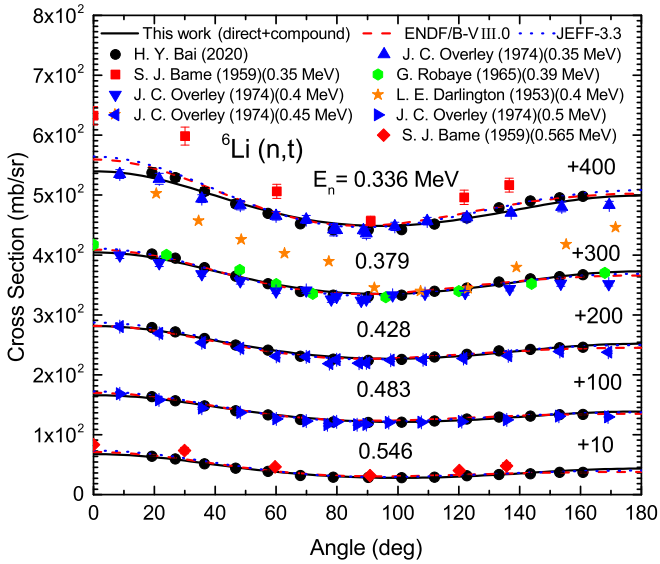

FIG. 28. The same as Fig. 7 but for different incident energies and different experimental data [9,91,92,94,95] as labeled in this figure.

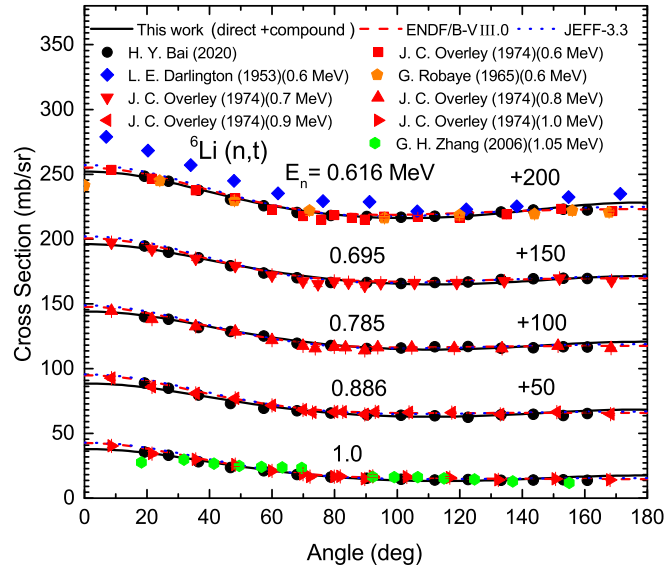

FIG. 29. The same as Fig. 7 but for different incident energies and different experimental data [9,81,91,94,95] as labeled in this figure.

ergy above 0.234 MeV, the comparisons of the calculated results with the experimental data are considerably improved, whereas the calculated results below 0.234 MeV are barely changed. Obviously, there are almost uniform agreements between calculated results and experimental data in the energy range from 0.298 to 1.0 MeV.

IV. SUMMARY AND CONCLUSION

With the combination of an effective excited energy formula proposed in this paper, the knockout process and heavy-particle knockout process based on zero-range DWBA theory well reproduced most of the available experimental data for the differential cross sections and angle-integrated cross sections of the emitted triton for the neutron-induced ^{6}Li reaction in the energy range from 1.0 eV to 3.0 MeV. The effects of the energy levels of the compound nucleus were reasonably taken into account. The weighting coefficients illustrating the relative contributions from the knockout process and heavy-particle knockout process, were determined by fitting the recent experimental data [9]. Furthermore, we found that the weighting coefficients could be expressed as a cubic function of energy. The shapes of the measured angular distributions in the energy range from 0.1 to 1.0 MeV were successfully explained by a tentative method through considering the contribution from the Hauser-Feshbach model. This investigation indicates that the ^{6}Li(n,t) reaction at low incident neutron energies still proceeds mainly through the direct reaction process, and the effects of the energy levels of the compound nucleus must be considered in the theoretical calculation. However, the contribution from the equilibrium reaction should not be ignored in the incident neutron energy range from 0.1 to 1.0 MeV. These theoretical methods are expected to analyze other light nucleus reactions at low energies.

ACKNOWLEDGMENTS

We thank N. Wang, L. Ou, M. Liu, H. Y. Peng, Y. Liang, X. D. Sun, X. F. Wu, C. Zhang, and Y. X. Qi for some valuable suggestions. This work was supported by the National Natural Science Foundation of China (Grants No. 12065003 and No. 11775166) and the Natural Science Foundation of Guangxi (Grant No. 2019GXNSFDA185011).

[1] G. H. Zhang *et al.*, Nucl. Instrum. Methods Phys. Res., Sect. A **566**, 615 (2006).
[2] M. Devlin *et al.*, *International Conference on Nuclear Data for Science and Technology, Nice, France, 2007* (EDP, Les Ulis, France, 2008), p. 1243.
[3] X. J. Sun and J. S. Zhang, EPJ Web Conf. **146**, 12026 (2017).
[4] X. J. Sun and J. S. Zhang, Phys. Rev. C **93**, 014609 (2016).
[5] J. S. Zhang, *Statistical Theory of Neutron Induced Reactions of Light Nuclei*, 2nd ed. (Science, Beijing, 2015) [in Chinese].
[6] J. Hu, X. Sun, J. Zhang, S. Wang, and Y. Han, Phys. Rev. C **101**, 034616 (2020).
[7] J. S. Zhang and Y. L. Han, Commun. Theor. Phys. **36**, 437 (2001).
[8] V. Semkova *et al.*, EPJ Web Conf. **146**, 07003 (2017).
[9] H. Y. Bai *et al.*, Chin. Phys. C **44**, 014003 (2020).
[10] G. M. Hale, Nucl. Data Sheets **109**, 2812 (2008).
[11] D. A. Brown *et al.*, Nucl. Data Sheets **148**, 1 (2018).
[12] M. A. Kellett and O. Bersillon, EPJ Web Conf. **146**, 02009 (2017).
[13] K. Shibata *et al.*, J. Nucl. Sci. Technol. **48**, 1 (2011).
[14] S. Chiba and K. Shibata, JAERI-M 88-164 (1988).
[15] G. M. Hale and H. M. Hofmann, in *International Conference on Nuclear Data for Science and Technology*, edited by R. C. Haight, M. B. Chadwick, T. Kawano, and Patrick Talou, AIP Conf. Proc. No. 769 (AIP, New York, 2005), p. 75.
[16] H. Weigmann and P. Manakos, Z. Phys. A **289**, 383 (1979).

[17] P. D. Kunz *et al.*, Phys. Lett. B **112**, 5 (1982).
[18] R. M. Devries, J. L. Perrenoud, and I. Slaus, Nucl. Phys. A **188**, 449 (1972).
[19] T. Y. Li and S. K. Mark, Can. J. Phys. **47**, 257 (1969).
[20] J. F. Cavaignac, N. Longequeue, and T. Honda, Nucl. Phys. A **167**, 207 (1971).
[21] S. E. Abdel-Kariem, Turk. J. Phys. **30**, 1 (2006).
[22] A. A. Cowley, Int. J. Mod. Phys. E **28**, 1950050 (2019).
[23] S. Chiba *et al.*, J. Nucl. Sci. Technol. **22**, 771 (1985).
[24] S. Chiba *et al.*, Phys. Rev. C **58**, 2205 (1998).
[25] G. D. Putt, Nucl. Phys. A **161**, 547 (1971).
[26] A. A. Naqvi, M. N. Nagadi, S. Kidwai, Khateeb-ur-Rehman, Phys. Rev. C **65**, 054615 (2002).
[27] D. G. Gerke *et al.*, Nucl. Phys. **75**, 609 (1966).
[28] J. M. Lombaard and E. Friedland, Z. Physik. **268**, 413 (1974).
[29] R. V. Poore *et al.*, Nucl. Phys. A **92**, 97 (1967).
[30] P. W. Chudleigh, C. K. Gowers, and E. G. Muirhead, Nucl. Phys. A **123**, 114 (1969).
[31] J. Dabrowski and J. Sawicki, Phys. Rev. **97**, 1002 (1955).
[32] T. I. Kopaleishvili, Sov. Phys. JETP **6**, 606 (1958).
[33] T. S. Cheng, *Nuclear Physics for Low and Medium High Energy*, (Peking University Press, Beijing, 1997) [in Chinese].
[34] M. Y. M. Hassan, E. H. Ismail, and A. Rabie, Z. Phys. A: At. Nucl. **285**, 37 (1978).
[35] M. Tanifuji, Nucl. Phys. **40**, 357 (1963).
[36] D. R. Ober and O. E. Johnson, Phys. Rev. **170**, 924 (1968).
[37] B. B. Srivastava, S. W. Cosper, and O. E. Johnson, Phys. Rev. **153**, 1221 (1967).
[38] N. Burtebayev *et al.*, Nucl. Phys. A **909**, 20 (2013).
[39] G. Gambarini *et al.*, Nucl. Phys. A **126**, 562 (1969).
[40] T. Honda and H. Ui, Nucl. Phys. **34**, 593 (1962).
[41] T. Honda *et al.*, Phys. Lett. **10**, 99 (1964).
[42] T. Honda *et al.*, Nucl. Phys. **62**, 561 (1965).
[43] A. Corana *et al.*, ACM Trans. Math. Software **13**, 262 (1987).
[44] R. M. Young, *An Introduction to Nonharmonic Fourier Series*, (Academic, New York, 1980).
[45] G. R. Satcher, *Direct Nuclear Reaction*, (Oxford University Press, New York, 1983).
[46] G. R. Satcher, Nucl. Phys. **55**, 1 (1964).
[47] J. Y. Park, Prog. Theor. Phys. **30**, 45 (1963).
[48] D. R. Tilley *et al.*, Nucl. Phys. A **541**, 1 (1992).
[49] D. R. Tilley *et al.*, Nucl. Phys. A **708**, 3 (2002).
[50] D. R. Tilley *et al.*, Nucl. Phys. A **745**, 155 (2004).
[51] W. Hauser and H. Feshbach, Phys. Rev. **87**, 366 (1952).
[52] J. M. Blatt and L. C. Biedenharn, Rev. Mod. Phys. **24**, 258 (1952).
[53] Z. D. Su *et al.*, At. Energ. Sci. Technol. **13**, 445 (1979).
[54] F. D. Becchetti, Jr. and G. W. Greenlees, Phys. Rev. **182**, 1190 (1969).
[55] S. Kirkpatrick, C. D. Gelatt, Jr., and M. P. Vecchi, Science **220**, 671 (1983).
[56] G. C. Chen *et al.*, Nucl. Sci. Eng. **163**, 272 (2009).
[57] Q. B. Shen, Nucl. Sci. Eng. **141**, 78 (2002).
[58] Sh. Hamada, N. Burtebayev, and N. Amangeldi, Int. J. Mod. Phys. E **23**, 1450061 (2014).
[59] R. G. Lovas *et al.*, Nucl. Phys. A **474**, 451 (1987).
[60] A. M. Young, S. L. Blatt, and R. G. Seyler, Phys. Rev. Lett. **25**, 1764 (1970).
[61] E. Ventura, C. C. Chang, and W. E. Meyerhof, Nucl. Phys. A **173**, 1 (1971).
[62] V. N. Bragin *et al.*, Phys. Atom. Nucl. **44**, 312 (1986).
[63] N. Burtebaev *et al.*, Phys. Atom. Nucl. **58**, 540 (1995).
[64] I. V. Kurdyumov, V. G. Neudatchin, and Yu. F. Smirnov, Phys. Lett. B **31**, 426 (1970).
[65] W. Dollhopf *et al.*, Phys. Lett. B **58**, 425 (1975).
[66] D. Albrecht *et al.*, Nucl. Phys. A **338**, 477 (1980).
[67] R. G. H. Robertson, P. Dyer, R. A. Warner, R. C. Melin, T. J. Bowles, A. B. McDonald, G. C. Ball, W. G. Davies, and E. D. Earle, Phys. Rev. Lett. **47**, 1867 (1981).
[68] P. G. Roos *et al.*, Phys. Rev. C **15**, 69 (1977).
[69] P. G. Roos *et al.*, Nucl. Phys. A **257**, 317 (1976).
[70] G. R. Plattner, M. Bornand, and K. Alder, Phys. Lett. B **61**, 21 (1976).
[71] D. R. Lehman and M. Rajan, Phys. Rev. C **25**, 2743 (1982).
[72] V. I. Kukulin *et al.*, Nucl. Phys. A **417**, 128 (1984).
[73] R. Beck, F. Dickmann, and R. G. Lovas, Nucl. Phys. A **446**, 703 (1985).
[74] K. Varga and R. G. Lovas, Phys. Rev. C **43**, 1201 (1991).
[75] A. Csoto and R. G. Lovas, Phys. Rev. C **46**, 576 (1992).
[76] H. Walliser and Y. C. Tang, Phys. Lett. B **135**, 344 (1984).
[77] T. Yoshimura *et al.*, Nucl. Phys. A **641**, 3 (1998).
[78] N. Burtebaev *et al.*, Phys. Atom. Nucl. **59**, 29 (1996).
[79] L. E. Kirsch *et al.*, Nucl. Instrum. Methods Phys. Res., Sect. A **874**, 57 (2017).
[80] C. Romano *et al.*, Nucl. Instrum. Methods Phys. Res., Sect. A **562**, 771 (2006).
[81] G. H. Zhang *et al.*, Nucl. Sci. Eng. **153**, 41 (2006).
[82] G. H. Zhang *et al.*, Nucl. Sci. Eng. **143**, 86 (2003).
[83] M. Drosg, D. M. Drake, and J. Masarik, Nucl. Instrum. Methods Phys. Res., Sect. B **94**, 319 (1994).
[84] J. C. Engdahl, G. F. Knoll, and J. C. Robertson, Nucl. Sci. Eng. **78**, 44 (1981).
[85] C. M. Bartle, Nucl. Phys. A **330**, 1 (1979).
[86] R. L. Macklin, R. W. Ingle, and J. Halperin, Nucl. Sci. Eng. **71**, 205 (1979).
[87] G. P. Lamaze, R. A. Schrack, and O. A. Wasson, Nucl. Sci. Eng. **68**, 183 (1978).
[88] C. Renner *et al.*, Bull. Am. Phys. Soc. **23**, 526 (1978).
[89] C. Mahaux and G. Robaye, Nucl. Phys. **74**, 161 (1965).
[90] C. Beets *et al.*, Nucl. Phys. **69**, 145 (1965).
[91] J. C. Overley, R. M. Sealock, and D. H. Ehlers, Nucl. Phys. A **221**, 573 (1974).
[92] S. J. Bame Jr and R. L. Cubitt, Phys. Rev. **114**, 1580 (1959).
[93] Y. Baudinet-Robinet *et al.*, J. Phys. **24**, 803 (1963) [in French].
[94] L. E. Darlington *et al.*, Phys. Rev. **90**, 1049 (1953).
[95] G. Robaye, L. Winand, and J. M. Delbrouck-Habaru, European-American Nuclear Data Committee Documents, No. 50-S, 1, 18 (1965), http://www-nds.ciae.ac.cn/exfor/servlet/X4sDownloadPdf?x4coding=2&x4ref=R,EANDC-50-S,(1),(18),1965.
[96] J. B. Weddell and J. H. Roberts, Phys. Rev. **95**, 117 (1954).
[97] V. P. Perelygin and K. D. Tolstov, Journal of Nuclear Energy. Parts A/B. Reactor Science and Technology **16**, 497 (1962).
[98] M. Drosg, Nucl. Sci. Eng. **183**, 143 (2016).
[99] D. Rendic *et al.*, Zentralinst. f. Kernforschung Rossendorf Reports, No.130, p.143 (1967), http://www-nds.ciae.ac.cn/exfor/servlet/X4sDownloadPdf?x4coding=2&x4ref=R,ZFK-130,143,196712.
[100] A. Trkov and D. A. Brown, Brookhaven National Laboratory Report No. BNL-203218-2018-INRE, 2018.